STRUCTURAL BIOLOGY
ISSN 2059-7983

Structural insight into industrially relevant glucoamylases: flexible positions of starch-binding domains

Christian Roth,[a]‡§ Olga V. Moroz,[a]‡ Antonio Ariza,[a]‡¶ Lars K. Skov,[b] Keiichi Ayabe,[c] Gideon J. Davies[a] and Keith S. Wilson[a]*

[a]Structural Biology Laboratory, Department of Chemistry, University of York, Heslington, York YO10 5DD, England, [b]Novozymes A/S, Krogshøjvej 36, DK-2880 Bagsværd, Denmark, and [c]Novozymes Japan Ltd, Chiba-shi 261-8501, Japan. *Correspondence e-mail: keith.wilson@york.ac.uk

Received 1 February 2018
Accepted 27 March 2018

Edited by R. J. Read, University of Cambridge, England

‡ The first three authors contributed equally to this work.
§ Current address: Carbohydrates: Structure and Function, Biomolecular Systems, Max Planck Institute of Colloids and Interfaces, Berlin, Germany.
¶ Current address: Sir William Dunn School of Pathology, University of Oxford, Oxford OX1 3RE, England.

Keywords: starch biomass degradation; glucoamylases; carbohydrate-binding module; *Penicillium oxalicum*; *Hormoconis resinae*; *Aspergillus niger*.

PDB references: *Penicillium oxalicum* glucoamylase, 6fhv; *Hormoconis resinae* glucoamylase, 6fhw; *Aspergillus niger* glucoamylase, 6frv

Supporting information: this article has supporting information at journals.iucr.org/d

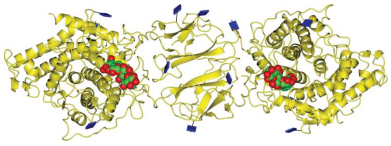

© 2018 International Union of Crystallography

Glucoamylases are one of the most important classes of enzymes in the industrial degradation of starch biomass. They consist of a catalytic domain and a carbohydrate-binding domain (CBM), with the latter being important for the interaction with the polymeric substrate. Whereas the catalytic mechanisms and structures of the individual domains are well known, the spatial arrangement of the domains with respect to each other and its influence on activity are not fully understood. Here, the structures of three industrially used fungal glucoamylases, two of which are full length, have been crystallized and determined. It is shown for the first time that the relative orientation between the CBM and the catalytic domain is flexible, as they can adopt different orientations independently of ligand binding, suggesting a role as an anchor to increase the contact time and the relative concentration of substrate near the active site. The flexibility in the orientations of the two domains presented a considerable challenge for the crystallization of the enzymes.

1. Introduction

Starch and glycogen comprise one of the major reserves of carbon and energy for all life. Furthermore, starch is one of the most important commodities for the food industry as well as for biofuel production (reviewed in Torney *et al.*, 2007; Lovegrove *et al.*, 2017). Owing to the high stability of the glycosidic bond (Wolfenden *et al.*, 1998) and the internal structure of starch, current industrial processes to modify and break it down usually require harsh conditions. In nature there are a huge variety of specialized enzymes that modify and degrade glycogen and raw starch (reviewed in Whelan, 1971). In contrast, in industry the non-enzymatic modification and breakdown of raw starch mostly requires harsh conditions that are not desirable in green environmentally friendly processes (Xu *et al.*, 2016). The use of enzymes proved to be a sustainable alternative to chemical processes and is now a multi-billion-dollar market (Chemier *et al.*, 2009). Among the most important classes of enzymes for the complete degradation of starch are glucoamylases, which are members of glycoside hydrolase family 15 (GH15; reviewed in CAZypedia at https://www.cazypedia.org/index.php/Glycoside_Hydrolase_Family_15; The CAZypedia Consortium, 2017) of the CAZy database (http://www.cazy.org; Lombard *et al.*, 2014) that catalyse the cleavage of α-1,4- and α-1,6-glycosidic bonds. Glucoamylases use a classical acid/base Koshland-type inverting mechanism,

releasing β-glucose from the nonreducing end of an α-glucan chain (Koshland, 1953; Weil *et al.*, 1954; Pazur & Ando, 1959, 1960). Fungal enzymes in particular are widely used for the complete degradation of starch to glucose (reviewed in Norouzian *et al.*, 2006), and early on their heavy use sparked high interest in the structural and functional characterization of microbial glucoamylases from a variety of sources (bacterial, fungal and eukaryotic). All glucoamylases possess a common catalytic domain, which can be followed or preceded by additional domains, usually carbohydrate-binding modules (CBMs; reviewed in Boraston *et al.*, 2004; Marín-Navarro & Polaina, 2011). The catalytic domain alone is able to degrade oligosaccharides, but the carbohydrate-binding domain proved to be essential for the interaction and degradation of raw starch (Stoffer *et al.*, 1993; Sauer *et al.*, 2000).

The first crystal structure of a glucoamylase was that of the catalytic domain of the *Aspergillus awamori* var. X100 glucoamylase (Aleshin *et al.*, 1992). The structure revealed a 13-α-helix fold with an $(\alpha/\alpha)_6$-helical bundle as the core, with the active site in a deep funnel-like structure at the N-terminal side of the helical bundle. A subsequent structure of a complex with the well known inhibitor acarbose allowed the identification of two conserved catalytic glutamic acid residues and important interactions in up to four well defined subsites (Aleshin *et al.*, 1994). The structure confirmed that glucoamylases employ a single-displacement mechanism with inversion of the anomeric centre, as first deduced by Weil *et al.* (1954). Insight into the interaction with raw starch was gained through various NMR and crystal structures of an isolated CBM alone and in complex with β-cyclodextrin or isomaltose (Sorimachi *et al.*, 1997; Chu *et al.*, 2014). The CBM forms a twisted β-sandwich domain and at least two different starch-binding sites have been identified in the *Aspergillus niger* CBM (Sorimachi *et al.*, 1997). The relative orientation of the catalytic domain and the CBM to one another and their interaction was studied using scanning tunnelling microscopy, suggesting an average distance of 90 Å and multiple different conformations (Kramer *et al.*, 1993; Sauer *et al.*, 2000). The first crystal structure of a full-length glucoamylase was solved from *Hypocrea jecorina* in 2008 (Bott *et al.*, 2008) and showed the CBM in a single orientation consistent with feeding an amylose chain into the active site. However, a single structure cannot reflect the flexible orientation observed using scanning tunnelling microscopy and light scattering that is thought to be important for the complete degradation of starch (Kramer *et al.*, 1993; Payre *et al.*, 1999).

Here, we have crystallized and determined the X-ray crystal structures of three industrially relevant glucoamylases. We describe the full-length structures of *Hormoconis resinae* GA (HrGA) and *Penicillium oxalicum* GA (PoGA) in their native states, as well as the catalytic domain of *A. niger* GA (AnGA). Two distinct relative conformations of the CBM were observed and reveal for the first time that multiple conformations are adopted independent of ligand binding. This advances our understanding of how glucoamylases interact with the substrate and subsequently degrade the starch polymer into its monomers.

2. Materials and methods

2.1. Cloning, expression and purification

The genes encoding the glucoamylases (UniProt accession Nos.: AnGA, P69328; HrGA, Q03045; PoGA, S7ZIW0) were cloned, expressed in *A. niger* and the proteins purified as described for PoGA by Li *et al.* (2010). Briefly, the culture broth from fermentation of *A. niger* MBin118 harbouring the glucoamylase gene was filtrated through a 0.22 µm PES filter and applied onto an α-cyclodextrin affinity gel column previously equilibrated with 50 m*M* sodium acetate, 150 m*M* NaCl pH 4.5 buffer. Unbound material was washed off the column with equilibration buffer and the glucoamylase was eluted using the same buffer containing 10 m*M* β-cyclodextrin over three column volumes. The glucoamylase activity of the eluate was checked to determine whether the glucoamylase had bound to the α-cyclodextrin affinity gel. The purified glucoamylase sample was then dialysed against 20 m*M* sodium acetate pH 5.0. The purity was finally checked by SDS–PAGE and only a single band was observed. Purified proteins were provided by Novozymes to the University of York. PoGA was further treated with Endo H to minimize N-glycosylation.

2.2. Crystallization

For all three proteins, initial crystallization screening was carried out using sitting-drop vapour diffusion with drops set up using a Mosquito Crystal liquid-handling robot (TTP Labtech, UK) with 150 nl protein solution plus 150 nl reservoir solution in 96-well format plates (MRC 2-well crystallization microplates, Swissci, Switzerland) equilibrated against 54 µl reservoir solution. Experiments were carried out at room temperature with a number of commercial screens. Crystallization of the intact proteins proved to be a challenge, presumably owing to microheterogenity as a result of non-uniform glycosylation.

2.2.1. *P. oxalicum* glucoamylase. Prior to crystallization, the protein was concentrated to 48 mg ml^{-1} by ultrafiltration in an Amicon centrifugation filter unit (Millipore) and aliquoted to 50 µl; aliquots that were not immediately set up for crystallization were flash-frozen in liquid nitrogen and stored at −80°C to use later in optimizations. The protein concentration was determined using a Coomassie (Bradford) assay (Bradford, 1976) with bovine serum albumin (BSA) as a standard. The protein was diluted to several concentrations in the range 10–48 mg ml^{-1} for the initial crystallization trials.

No hits appeared in the initial screens until an additional purification step by ion exchange was introduced. Anion exchange (the pI is 6.0) was carried out in 20 m*M* Tris–HCl pH 7.5, with shallow-gradient elution in 20 m*M* Tris–HCl pH 7.5, 1 *M* NaCl. The asymmetrical peak started eluting at 50 m*M* NaCl, the shoulder was separated from the main peak and fractions corresponding to the main peak were pooled and concentrated to 10 mg ml^{-1}.

Initial hits were obtained in PACT *premier* HT-96 (Molecular Dimensions), with the best hit being very small clusters in condition E8 (0.2 *M* sodium sulfate, 20% PEG 3350). Seeding stock was prepared from condition E8, and MMS

Table 1
Crystallization.

	PoGA	AnGA	HrGA
Method	Vapour diffusion, sitting drop, MMS	Vapour diffusion, sitting drop	Vapour diffusion, sitting drop
Plate type	MRC 2-well crystallization microplate, Swissci, Switzerland		
Temperature (K)	293	293	293
Protein concentration (mg ml^{-1})	10	18	37
Buffer composition of protein solution	20 m*M* Tris–HCl pH 7.5, 50 m*M* NaCl	25 m*M* piperazine pH 5.0, 150 m*M* NaCl	20 m*M* sodium acetate pH 5.0
Seeding-stock composition	PACT condition E8 (0.2 *M* sodium sulfate, 20% PEG 3350)	N/A	N/A
Composition of reservoir solution	PACT condition C1 [PCB (sodium propionate + sodium cacodylate + bis-tris-propane buffer pH 4.0), 25% PEG 1500] + 1/3 Silver Bullet condition G2 (0.2% thiodiglycolic acid, 0.2% adipic acid, 0.2% benzoic acid, 0.2% anhydrous oxalic acid, 0.2% terephthalic acid, 20 m*M* HEPES pH 6.8)	Index condition H8 (0.1 *M* HEPES pH 7.5, 25% PEG 3350)	Index condition C5 (60% Tacsimate pH 7.0)
Volume and ratio of drop	200 nl protein + 150 nl reservoir (100 nl screen condition + 50 nl Silver Bullets) + 50 nl seeding stock	150 nl protein + 150 nl reservoir	150 nl protein + 150 nl reservoir
Volume of reservoir (µl)	54	54	54

(microseed matrix screening; for a review, see D'Arcy *et al.*, 2014) was performed according to the published protocols (Shaw Stewart *et al.*, 2011). Briefly, crystals from the initial successful drop were transferred onto a glass slide, crushed and collected in a Seed Bead (Hampton Research) with 50 µl well solution added, vortexed for 1 min and used as an initial seeding stock: unused seeding stocks were stored at −20°C for later experiments. MMS was carried out with 150 nl protein solution plus 100 nl reservoir solution plus 50 nl seeding stock with a Mosquito Crystal liquid-handling robot, using the PACT *premier* HT-96 screen. Following MMS, the best hit was obtained in condition C1 [PCB (sodium propionate + sodium cacodylate + bis-tris-propane buffer pH 4.0), 25% PEG 1500]. These again were clusters of intergrown crystals, but were larger and better defined than the initial crystals. Final optimization was carried out using the Silver Bullets screen (Hampton Research), where different additives that have been found to be successful for various proteins in the past are added to the same 'hit' condition while seeding with the same seeding stock as before (PACT *premier* condition E8). This was successful and produced diffraction-quality crystals in condition G2 (0.2% thiodiglycolic acid, 0.2% adipic acid, 0.2% benzoic acid, 0.2% anhydrous oxalic acid, 0.2% terephthalic acid, 20 m*M* HEPES pH 6.8). To summarize, the condition that gave the final crystals was PACT *premier* condition C1 (100 nl) with added Silver Bullets condition G2 (50 nl) and seeding stock from PACT condition E8 (Table 1). The crystals were cryoprotected with PEG 1500, which was added to the crystallization condition to a final concentration of 34%. Data were collected on Diamond Light Source beamline I04-1 to 2.0 Å resolution. The data were indexed and integrated with *XDS* (Kabsch, 2010) and subsequently scaled and merged with *AIMLESS* (Evans & Murshudov, 2013).

2.2.2. *A. niger* glucoamylase. A number of hits appeared in the initial screens, with a single crystal suitable for diffraction being obtained in condition H8 of the Index screen (Hampton Research): 0.1 *M* HEPES pH 7.5, 25% PEG 3350. Without further cryoprotection, owing to the presence of 25% PEG, the crystals were flash-cooled in liquid nitrogen and data were collected on beamline ID14-1 at the ESRF to a resolution of 2.3 Å. However, the diffraction was of limited quality, with streaking of the spots, some evidence of splitting and possible ice rings. In addition, after structure solution the crystal, as described below, only contained the catalytic domain of the protein. X-ray data were processed with *XDS* (Kabsch, 2010), followed by *AIMLESS* (Evans & Murshudov, 2013) for scaling and merging.

2.2.3. *H. resinae* glucoamylase. The protein was co-crystallized with 7.5 m*M* acarbose. Large orthogonal crystals formed in condition C5 of the Index screen (60% Tacsimate pH 7.0), the best of which diffracted to 6 Å resolution at a home source (Rigaku MicroMax-007 HF rotating anode) using 25% glycerol as a cryoprotectant. Data were collected on beamline ID14-2 at the ESRF to a maximum resolution of 3.6 Å, processed with *MOSFLM* (Leslie, 2006) and scaled with *AIMLESS* (Evans & Murshudov, 2013).

Data-processing statistics for all three enzymes are given in Table 2.

2.3. Structure solution and refinement

The structures were solved by molecular replacement using *Phaser* (McCoy *et al.*, 2007) with the catalytic domain of *A. awamori* GA as a search model (PDB entry 1glm; Aleshin *et al.*, 1994). The solution of AnGA was problematical. The images were initially integrated in space group *P*1, while the intensity statistics suggested that the crystal was twinned. Merging the data and refining the model was attempted in space group *P*1 with four molecules per asymmetric unit, in $P2_1$ with two molecules per asymmetric unit and in $P2_12_12_1$ with a single molecule in the asymmetric unit: for each of these the refined R and $R_{\rm free}$ were around 25% and 32%,

Table 2
Data collection and processing.

Values in parentheses are for the outer shell.

	PoGA	AnGA	HrGA
Diffraction source	I04-1, Diamond Light Source	ID14-1, ESRF	ID14-2, ESRF
Wavelength (Å)	0.9173	0.9334	0.933
Temperature (K)	100	100	100
Detector	PILATUS 2M	ADSC Q210 CCD	ADSC Q210 CCD
Crystal-to-detector distance (mm)	222.7	227.2	307.5
Rotation range per image (°)	0.2	0.5	1.0
Total rotation range (°)	180	180	121
Exposure time per image (s)	0.2	3	10
Space group	*H*32	$P2_12_12_1$	$P2_12_12_1$
a, *b*, *c* (Å)	189.3, 189.3, 115.4	56.4, 73.1, 102.9	138.0, 149.8, 192.4
α, β, γ (°)	90, 90, 120	90, 90, 90	90, 90, 90
Mosaicity (°)	0.24	1.13	1.53
Resolution range (Å)	47.31–2.00 (2.05–2.00)	44.64–2.30 (2.38–2.30)	59.98–3.60 (3.76–3.60)
Total No. of reflections	548252 (35057)	138362 (13756)	248567 (25376)
No. of unique reflections	53301 (3921)	19454 (1870)	38033 (3798)
Completeness (%)	100 (100)	99.5 (99.9)	81.8 (68.0)
Multiplicity	10.3	7.1 (7.4)	6.5 (5.5)
$\langle I/\sigma(I)\rangle$	6.2 (1.0)†	6.3 (1.3)	10.5 (2.5)
$R_{r.i.m.}$‡	0.225 (2.284)	0.071 (0.556)	0.142 (0.675)
$CC_{1/2}$	0.994 (0.394)	0.995 (0.816)	0.994 (0.889)
Overall *B* factor from Wilson plot (Å^2)	28.3	36.16	45.0

† The value of $CC_{1/2}$ is 0.394 for PoGA and 0.816 for AnGA in the highest resolution shell, outside the usually accepted level, which reflects the paucity of data at the limited resolution of these structures. Consistent with this, $\langle I/\sigma(I)\rangle$ drops below 2.0 at a resolution of 2.18 Å for PoGA and 2.58 Å for AnGA. ‡ Redundancy-independent merging *R* factor $R_{r.i.m}$ (Diederichs & Karplus, 1997).

respectively. It was therefore decided to use the higher symmetry orthorhombic space group for the analysis, while accepting that the data and refinement statistics are poor for a structure at this resolution. Fortunately, the AnGA structure is of least importance to the conclusions of this work, since it lacks the starch-binding domain, and another structure of the catalytic domain solved at higher resolution is already available (Lee & Paetzel, 2011). For HrGA and PoGA additional unexplained density was attributed to the CBM, which was subsequently placed by an additional round of molecular replacement using the CBM from *H. jecorina* (PDB entry 2vn4; Bott *et al.*, 2008) as a model. The structures were subsequently rebuilt in real space using *Coot* (Emsley *et al.*, 2010) followed by reciprocal-space refinement with *REFMAC* (Murshudov *et al.*, 2011) within *CCP*4*i*2 (Potterton *et al.*, 2018). The respective glycosylation was added in *Coot* and refined in *REFMAC* using dictionaries created with *Privateer* (Agirre *et al.*, 2015). The dictionaries allowed the use of additional monoperiodic torsion restraints to stabilize the conformation of the carbohydrate rings. All other linker parameters were taken from the *CCP*4 monomer library. The quality of the final models was evaluated using *MolProbity* (Chen *et al.*, 2010) as part of the *PHENIX* package (Adams *et al.*, 2011) and *Privateer*. Figures of the structural models were prepared with

Table 3
Structure solution and refinement.

	PoGA	AnGA	HrGA
PDB code	6fhv	6frv	6fhw
Resolution range (Å)	47.31–2.00	44.64–2.30	59.58–3.60
Completeness (%)	100	99.6	81.8
No. of reflections, working set	53296	19520	37085
No. of reflections, test set	2614	974	1887
Final R_{cryst}	18.7	25.1	23.6
Final R_{free}	22.0	34.2	25.4
Cruickshank DPI	0.15	0.57	
No. of non-H atoms			
Protein	4576	3542	8959
Ligand	120	64	429
Water	257	27	
Total	5403	3633	9388
R.m.s. deviations			
Bonds (Å)	0.015	0.009	0.010
Angles (°)	1.63	1.27	1.68
Average *B* factors (Å^2)			
Protein	24.1	58.0	55.0
Ligand	44.7	60.0	83.6
Water	37.0	40.7	
Ramachandran plot			
Most favoured (%)	96.4	91.3	91.2
Allowed (%)	3.6	7.6	8.2

CCP4mg (McNicholas *et al.*, 2011). The final refinement statistics are given in Table 3.

3. Results

3.1. Crystallization and structure determination

Purified recombinantly expressed glucoamylases from the three organisms were crystallized in either a glycosylated form for AnGA and HrGA or a deglycosylated form in the case of PoGA. Data were collected to 2.0 Å resolution for the partially deglycosylated PoGA, to 2.3 Å resolution for AnGA and to 3.6 Å resolution for the glycosylated HrGA. The structures were solved by molecular replacement using the catalytic domain of *A. awamori* glucoamylase. Initial refinement revealed additional density for the linker region in all three structures, as well as for several N- and O-glycosylation sites. Surprisingly, the CBM in *A. niger* could not be seen, and closer inspection of the crystal packing indicated that the CBM cannot be accommodated in the crystal lattice and was probably cleaved off during crystallization. For the other two structures the full CBM could be built. The final model of AnGA includes one protein molecule in the asymmetric unit with residues 25–491 built and three *N*-acetylglucosamine molecules and two mannose residues as part of the N- and O-glycosylation sites, and was refined to a final *R* and R_{free} of 25.1% and 34.3%, respectively. The PoGA model included one molecule in the asymmetric unit comprising residues 30–616, three N-glycosylation sites, a bis-tris-propane (BTP) molecule and two PEG molecules, and was refined to an *R* and R_{free} of 18.7% and 22.0%, respectively. The HrGA model with two molecules in the asymmetric unit included residues 29–616 and up to seven N-glycosylation sites and had acarbose bound in the active site. The model was refined to an *R* and R_{free} of 23.8% and 25.4%, respectively.

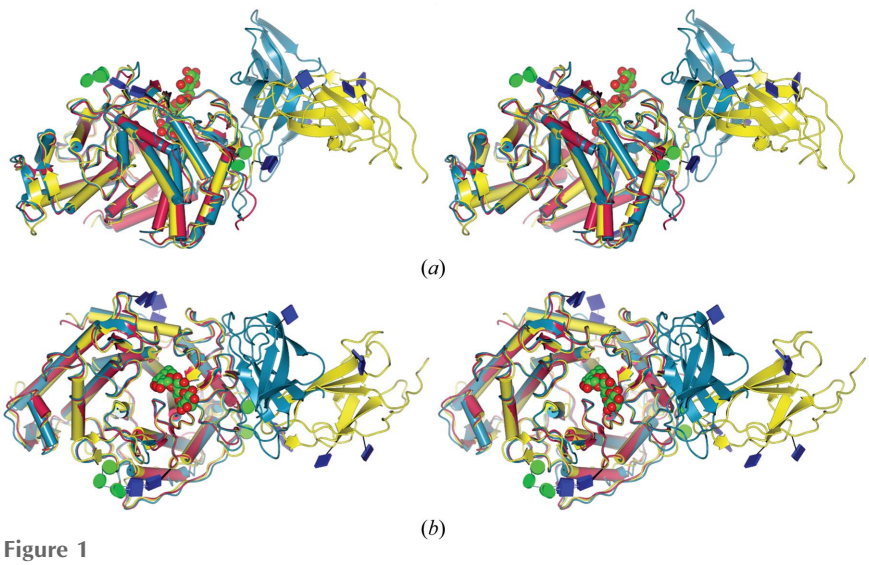

Figure 1
Stereo ribbon diagram of the tertiary structure of GA. (*a*) Side views of AnGA (red), HrGA (yellow) and PoGA (blue) with the relative domain orientation of the CBMs of HrGA and PoGA. The active site is indicated with acarbose, as observed in HrGA, in sphere representation. The corresponding glycosylation sites are shown as Glycoblocks (McNicholas & Agirre, 2017) coloured according to the residue type. The superposition is based on secondary-structure superposition of the catalytic domains. (*b*) Top view along the $(\alpha/\alpha)_6$-barrel.

3.2. Overall structure

The catalytic domains of all three structures superimpose with an r.m.s.d. of 1.2 Å over a maximum of 452 residues, despite an overall low sequence identity of approximately 50% (Fig. 1, Supplementary Fig. S1). The domain follows the canonical fold with an $(\alpha/\alpha)_6$-barrel. In all three structures the part of the linker domain that interacts with the catalytic domain is structurally conserved.

The C-terminal CBM adopts the well known β-sandwich motif, which is a hallmark of carbohydrate-binding modules. A sequence comparison classifies the CBMs of both HrGA and PoGA into CAZy family CBM20 (Boraston *et al.*, 2004; Lombard *et al.*, 2014). In addition, the CBMs of HrGA and PoGA adopt two different relative conformations with respect to the catalytic domain, with concomitant differences in the position of the C-terminal part of the linker (Fig. 1). Owing to the different positions HrGA has an extended arrangement of both domains, whereas PoGA adopts an overall more compact structure.

3.3. Protein glycosylation

3.3.1. N-Glycosylation. The catalytic domain of AnGA has two resolved N-glycosylation sites at Asn195 and Asn419, with two GlcNAc residues visible at Asn195 and one at Asn419.

The full-length structures of HrGA and PoGA show a greater degree of N-glycosylation, which is most extensive for HrGA, where the resolved sites are at Asn99, Asn200, Asn427, Asn500, Asn514, Asn528 and Asn587. Asn200 is the only site that shows branching of the glycosylation chain. In PoGA three glycosylation sites at Asn184, Asn410 and Asn514 are observed. The most extensive at Asn184 is structurally equivalent to Asn200 in HrGA and Asn195 in AnGA.

3.3.2. O-Glycosylation. O-Glycosylation was only observed in AnGA, in particular in the linker domain, which would connect to the CBM. Only two sites, at Ser483 and Ser484, could be modelled with confidence.

3.4. Inhibitor binding

HrGA was co-crystallized with the well known inhibitor acarbose. Clear density corresponding to the inhibitor was found in the active sites of both independent monomers. In both monomers an acarbose molecule was fitted and refined, assuming full occupancy. The resulting average *B* value of 41.3 Å^2 is similar to those for the surrounding residues and supports the full occupancy. The inhibitor occupies the active-site pocket with the cyclohexitol moiety of acarviosine populating the −1 subsite. [For subsite nomenclature, see Davies *et al.* (1997); briefly, subsites are labelled from $-n$ to $+n$, with $-n$ at the nonreducing end and $+n$ at the reducing end. Cleavage occurs between the −1 and +1 subsites.] There are further interactions with the sugars in subsite +1 (4-amino-4,6-deoxyglucose) and +2 (glucose), whereas the terminal sugar is not stabilized by direct interactions with the protein. The inhibitor interacts with HrGA by multiple hydrogen bonds and hydrophobic interactions with conserved residues in the active site (Supplementary Fig. S2). The catalytic acid Glu208 forms a hydrogen bond to the bridging N atom in acarbose as expected for a productive complex with a substrate having a glycosidic bond.

The catalytic base Glu432 is at a distance of 3.9 Å from the anomeric C atom, but is hydrogen-bonded to Tyr76. The PoGA substrate-binding site is occupied by a BTP molecule, which was part of the crystallization medium, which spans subsites −1 and +1 with multiple hydrogen bonds, including to the catalytic acid. The BTP molecule refines with an average *B* value of 38 Å^2 at full occupancy, which is similar to those of the surrounding residues. In AnGA the active site is empty. There are no significant shifts of the side chains lining the active site between the three structures, indicating a rigid active site.

4. Discussion

The structures of the three glucoamylases show a high degree of conservation in the catalytic domain, as well as for the part of the linker which interacts with the catalytic domain. Whereas the CBM domain was missing in AnGA, a full-length model could be built for HrGA and PoGA.

In the active site of HrGA, one acarbose molecule was identified. The residues that interact with acarbose are

identical to those described for *A. awamori* GA (Aleshin *et al.*, 1994), with the catalytic acid Glu208 interacting with the imino linkage of acarbose and Glu432, the catalytic base, approximately 4 Å away. The arrangement and distance between the two catalytic residues support the proposed inverting mechanism for these enzymes (Weil *et al.*, 1954; Pazur & Ando, 1959, 1960; McCarter & Withers, 1994). In PoGA a BTP molecule was modelled into the active site, forming key interactions with residues in subsites −1 and +1. A similar situation was observed for the structure of the catalytic domain of AnGA (Lee & Paetzel, 2011), in which a Tris and a glycerol molecule were found in subsites −1 and +1, respectively. Tris and its derivatives are well known inhibitors of glycoside hydrolases (Roberts & Davies, 2012), which has even led to the development of inhibitors sharing common characteristics (Taylor *et al.*, 2007).

All three structures reveal several glycosylation sites in the N-terminal domain, as well as in the CBM for PoGA and HrGA. The N-glycosylation sites are highly conserved, suggesting a functional role, for example in protein secretion or stability. The N-glycosylation site in AnGA at Asn195 corresponds to Asn184 in PoGA and Asn200 in HrGA, and shows the highest degree of complexity of all sites in the latter two glucoamylases. Residual density suggests additional sugars in AnGA at this site, but the quality of the electron density did not allow further extension of the glycosylation tree. This site is close to the linker connecting the CBM and might be of special importance for the stability of the linker. The importance of this site is further supported by the fact that treatment of PoGA with Endo H still left this site intact. The N-glycosylation sites at Asn528 and Asn587 in the CBM of HrGA are in close proximity to the proposed starch-binding site 1 in the AnGA CBM (Sorimachi *et al.*, 1997), suggesting that only binding site 2 is involved in interaction with the substrate in HrGA.

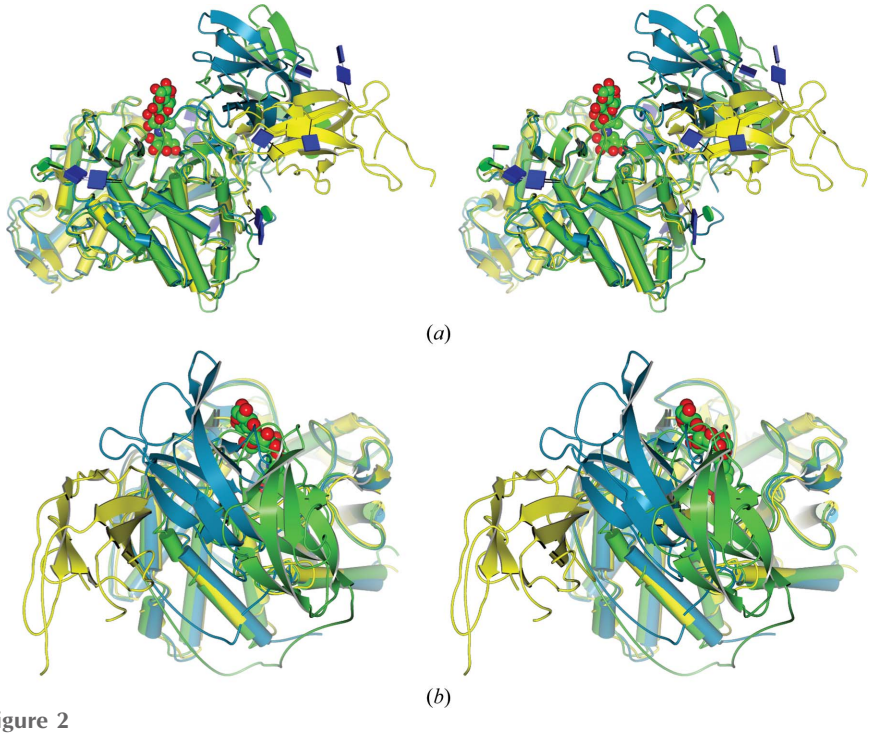

Figure 2
Stereo representation of the relative orientation of the CBM with respect to the catalytic domain from the side (*a*) and from the front (*b*). HrGA is coloured in yellow, PoGA in blue and HjGA (PDB entry 2vn7) in green. The active site is indicated with acarbose in sphere representation. The glycosylation sites are shown as Glycoblocks (McNicholas & Agirre, 2017) coloured according to the residue type.

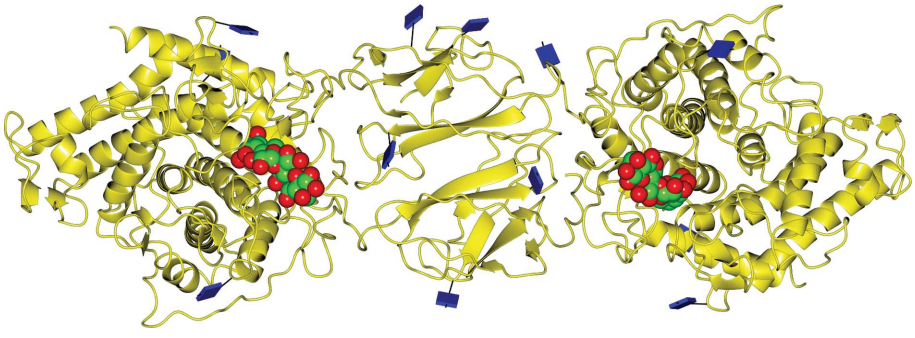

Figure 3
Potential dimer of HrGA determined from the crystal structure using *PISA* (Krissinel, 2015). The bound inhibitor acarbose is shown in sphere representation, whereas the glycosylation is shown as Glycoblocks (McNicholas & Agirre, 2017).

Interestingly, O-glycosylation was only found in AnGA, specifically in the linker region. Although more sites are known (Lee & Paetzel, 2011), only two (Ser483 and Ser484) could be modelled with confidence. Another model, refined to higher resolution, showed up to seven glycosylation sites, with an eighth suggested but not modelled (Lee & Paetzel, 2011). The role of this specific linker glycosylation is not known, but a role in protein stability has been proposed (Goto *et al.*, 1997). Additionally, it was shown that the extent of O-glycosylation influences the susceptibility of AnGA to proteolytic degradation, which decreases with higher glycosylation (Le Gal-Coëffet *et al.*, 1995).

The potential variability in the glycosylation pattern might also explain the positive effect of the fine-tuning of ion-exchange purification on crystallization, which is in agreement with the suggestion that the protein naturally occurs as multiple species, owing to possible glycosylation micro-heterogenity and/or conformational variability, resulting in slight variations in the overall surface charge. Selecting a

species with homogenous surface charge by separating a narrow peak fragment facilitated the formation of crystal contacts that are favourable for crystallization.

Of particular interest in this study is the CBM domain (CAZy family CBM20) and its role in the degradation of raw starch. For both HrGA and PoGA, the CBM linked to the catalytic domain could be clearly modelled, with both domains forming a β-sandwich, a well known structural motif for CBMs. Glycoside hydrolase structures with intact appended CBMs are extremely rare, and are rarer still if connected by a flexible linker. It is therefore difficult to know whether these rare observations reflect a unique orientation or one favoured by a certain crystal-packing environment. Therefore, the most important observation is that the CBM domains in the two structures reported here adopt very different relative orientations with respect to the catalytic domain (Fig. 2) and to the orientation observed in the crystal structure of *H. jecorina* GA (HjGA) solved independently (Bott *et al.*, 2008). Whereas HrGA adopts a more extended structure with the two domains separated, PoGA adopts a rather compact arrangement. A flexible arrangement with different relative conformations for the CBM was previously proposed based on single-molecule scanning tunnelling microscopy and light-scattering data collected for AnGA (Kramer *et al.*, 1993; Payre *et al.*, 1999), which suggested that the average distance between the two domains is about 90 Å (Kramer *et al.*, 1993), corresponding to a rather extended arrangement. However, it has been proposed that a closer distance is necessary for proper function (Payre *et al.*, 1999). Indeed, dynamic light-scattering experiments pointed to a hydrodynamic radius of between 60 and 75 Å upon ligand binding (Payre *et al.*, 1999). The structure of HjGA was solved independently in two different crystal forms, with both domains in close proximity (Bott *et al.*, 2008), and these authors concluded that the compact conformation is the dominant active conformation. Further support for this model comes from the fact that this would bring the second CBM substrate-binding site close to the active site. A model with amylose as a substrate was developed, which takes advantage of the close proximity of the second substrate-binding site in CBM and the active site in the catalytic module (Bott *et al.*, 2008). Such a compact conformation is also supported by heterobifunctional inhibitors that can bridge the catalytic site and the CBM binding site (Payre *et al.*, 1999; Sauer *et al.*, 2000). Furthermore, multiple salt bridges and hydrophobic interactions have been proposed to stabilize this conformation. Nevertheless, compared with HjGA, the CBM in HrGa is in a conformation in which the proposed starch-binding site is remote from the active site, despite co-crystallization with acarbose. Comparing the compact conformation of PoGA with HjGA shows that the CBM in PoGA is in a more elevated position relative to the catalytic domain (Fig. 2), and in addition is also stabilized by multiple hydrogen bonds and hydrophobic interactions. Furthermore, no GA-specific inhibitor was present during the crystallization, although a bis-tris-propane buffer molecule was identified in the active site, which might be a weak inhibitor of GAs (Roberts & Davies, 2012). Taken together, all of the results gathered on different GAs point to the conclusion that the precise orientation of the CBM with respect to the catalytic domain is neither important, nor stabilized by specific interactions between the domains, nor favoured by the binding of inhibitors in the active site, and therefore does not influence the activity. Furthermore, GA variants with different linker lengths showed virtually no difference in activity provided that the linker has a minimal length of 17 residues to prevent steric clashes between the two domains (Sauer *et al.*, 2001). Additionally, the issue still engenders controversy owing to an alternative model, involving an extended conformation and subsequent dimerization, based on the results of small-angle X-ray scattering (SAXS) of AnGA (Jørgensen *et al.*, 2008). Indeed, analysis of the potential stable oligomers in the crystal revealed a dimer for HrGA with the two CBMs forming part of the interface (Fig. 3), showing some resemblance to the proposed SAXS model.

In summary, we solved the crystal structures of three industrially relevant glucoamylases, with two in the intact two-domain form. We show for the first time that the carbohydrate-binding module can adopt multiple relative orientations with respect to the catalytic module, independent of a bound ligand in the active site. The results are in agreement with single-molecule data and kinetic analysis of linker variants. Nevertheless, further research is needed to clarify the mode of action with respect to the synergy of binding and oligomerization on raw starch. Taken together, the data strongly indicate that many relative orientations are accessible in solution and contribute to the enhanced activity towards polymeric substrate by increasing the relative local substrate concentration and the probability of contact with the substrate, and may allow the catalytic domain to reach multiple structurally weak points in starch without dissociation from the substrate.

5. Related literature

The following references are cited in the Supporting Information for this article: Bond & Schüttelkopf (2009) and Edgar (2004).

Acknowledgements

We thank the ESRF for the access to beamlines ID14-1 and ID14-2, and Diamond Light Source for the access to beamline I04-1 (proposal No. mx-1221) that contributed to the results presented here. The authors also thank Dr Johan Turkenburg and Sam Hart for assistance during data collection.

References

Adams, P. D. *et al.* (2011). *Methods*, **55**, 94–106.
Agirre, J., Iglesias-Fernández, J., Rovira, C., Davies, G. J., Wilson, K. S. & Cowtan, K. D. (2015). *Nature Struct. Mol. Biol.* **22**, 833–834.
Aleshin, A. E., Firsov, L. M. & Honzatko, R. B. (1994). *J. Biol. Chem.* **269**, 15631–15639.
Aleshin, A., Golubev, A., Firsov, L. M. & Honzatko, R. B. (1992). *J. Biol. Chem.* **267**, 19291–19298.
Bond, C. S. & Schüttelkopf, A. W. (2009). *Acta Cryst.* D**65**, 510–512.

Boraston, A. B., Bolam, D. N., Gilbert, H. J. & Davies, G. J. (2004). *Biochem. J.* **382**, 769–781.

Bott, R., Saldajeno, M., Cuevas, W., Ward, D., Scheffers, M., Aehle, W., Karkehabadi, S., Sandgren, M. & Hansson, H. (2008). *Biochemistry*, **47**, 5746–5754.

Bradford, M. M. (1976). *Anal. Biochem.* **72**, 248–254.

Chemier, J. A., Fowler, Z. L., Koffas, M. A. & Leonard, E. (2009). *Adv. Enzymol. Relat. Areas Mol. Biol.* **76**, 151–217.

Chen, V. B., Arendall, W. B., Headd, J. J., Keedy, D. A., Immormino, R. M., Kapral, G. J., Murray, L. W., Richardson, J. S. & Richardson, D. C. (2010). *Acta Cryst.* D**66**, 12–21.

Chu, C.-H., Li, K.-M., Lin, S.-W., Chang, M. D.-T., Jiang, T.-Y. & Sun, Y.-J. (2014). *Proteins*, **82**, 1079–1085.

D'Arcy, A., Bergfors, T., Cowan-Jacob, S. W. & Marsh, M. (2014). *Acta Cryst.* F**70**, 1117–1126.

Davies, G. J., Wilson, K. S. & Henrissat, B. (1997). *Biochem. J.* **321**, 557–559.

Diederichs, K. & Karplus, P. A. (1997). *Nature Struct. Biol.* **4**, 269–275.

Edgar, R. C. (2004). *Nucleic Acids Res.* **32**, 1792–1797.

Emsley, P., Lohkamp, B., Scott, W. G. & Cowtan, K. (2010). *Acta Cryst.* D**66**, 486–501.

Evans, P. R. & Murshudov, G. N. (2013). *Acta Cryst.* D**69**, 1204–1214.

Goto, M., Ekino, K. & Furukawa, K. (1997). *Appl. Environ. Microbiol.* **63**, 2940–2943.

Jørgensen, A. D., Nøhr, J., Kastrup, J. S., Gajhede, M., Sigurskjold, B. W., Sauer, J., Svergun, D. I., Svensson, B. & Vestergaard, B. (2008). *J. Biol. Chem.* **283**, 14772–14780.

Kabsch, W. (2010). *Acta Cryst.* D**66**, 125–132.

Koshland, D. E. (1953). *Biol. Rev.* **28**, 416–436.

Kramer, G. F. H., Gunning, A. P., Morris, V. J., Belshaw, N. J. & Williamson, G. (1993). *Faraday Trans.* **89**, 2595–2602.

Krissinel, E. (2015). *Nucleic Acids Res.* **43**, W314–W319.

Lee, J. & Paetzel, M. (2011). *Acta Cryst.* F**67**, 188–192.

Le Gal-Coëffet, M.-F., Jacks, A. J., Sorimachi, K., Williamson, M. P., Williamson, G. & Archer, D. B. (1995). *Eur. J. Biochem.* **233**, 561–567.

Leslie, A. G. W. (2006). *Acta Cryst.* D**62**, 48–57.

Li, M., Duan, J., Liu, Z., Fukuyama, S., Ayabe, K., Coward-Kelly, G. & Deinhammer, R. (2010). Patent WO 2011127802 A1.

Lombard, V., Golaconda Ramulu, H., Drula, E., Coutinho, P. M. & Henrissat, B. (2014). *Nucleic Acids Res.* **42**, D490–D495.

Lovegrove, A., Edwards, C. H., De Noni, I., Patel, H., El, S. N., Grassby, T., Zielke, C., Ulmius, M., Nilsson, L., Butterworth, P. J., Ellis, P. R. & Shewry, P. R. (2017). *Crit. Rev. Food Sci. Nutr.* **57**, 237–253.

Marín-Navarro, J. & Polaina, J. (2011). *Appl. Microbiol. Biotechnol.* **89**, 1267–1273.

McCarter, J. D. & Withers, S. G. (1994). *Curr. Opin. Struct. Biol.* **4**, 885–892.

McCoy, A. J., Grosse-Kunstleve, R. W., Adams, P. D., Winn, M. D., Storoni, L. C. & Read, R. J. (2007). *J. Appl. Cryst.* **40**, 658–674.

McNicholas, S. & Agirre, J. (2017). *Acta Cryst.* D**73**, 187–194.

McNicholas, S., Potterton, E., Wilson, K. S. & Noble, M. E. M. (2011). *Acta Cryst.* D**67**, 386–394.

Murshudov, G. N., Skubák, P., Lebedev, A. A., Pannu, N. S., Steiner, R. A., Nicholls, R. A., Winn, M. D., Long, F. & Vagin, A. A. (2011). *Acta Cryst.* D**67**, 355–367.

Norouzian, D., Akbarzadeh, A., Scharer, J. M. & Moo Young, M. (2006). *Biotechnol. Adv.* **24**, 80–85.

Payre, N., Cottaz, S., Boisset, C., Borsali, R., Svensson, B., Henrissat, B. & Driguez, H. (1999). *Angew. Chem. Int. Ed.* **38**, 974–977.

Pazur, J. H. & Ando, T. (1959). *J. Biol. Chem.* **234**, 1966–1970.

Pazur, J. H. & Ando, T. (1960). *J. Biol. Chem.* **235**, 297–302.

Potterton, L. *et al.* (2018). *Acta Cryst.* D**74**, 68–84.

Roberts, S. M. & Davies, G. J. (2012). *Methods Enzymol.* **510**, 141–168.

Sauer, J., Christensen, T., Frandsen, T. P., Mirgorodskaya, E., McGuire, K. A., Driguez, H., Roepstorff, P., Sigurskjold, B. W. & Svensson, B. (2001). *Biochemistry*, **40**, 9336–9346.

Sauer, J., Sigurskjold, B. W., Christensen, U., Frandsen, T. P., Mirgorodskaya, E., Harrison, M., Roepstorff, P. & Svensson, B. (2000). *Biochim. Biophys. Acta*, **1543**, 275–293.

Shaw Stewart, P. D., Kolek, S. A., Briggs, A. R., Chayen, N. E. & Baldock, P. F. M. (2011). *Cryst. Growth Des.* **11**, 3432–3441.

Sorimachi, K., Le Gal-Coëffet, M. F., Williamson, G., Archer, D. B. & Williamson, M. P. (1997). *Structure*, **5**, 647–661.

Stoffer, B., Frandsen, T. P., Busk, P. K., Schneider, P., Svendsen, I. & Svensson, B. (1993). *Biochem. J.* **292**, 197–202.

Taylor, E. A., Clinch, K., Kelly, P. M., Li, L., Evans, G. B., Tyler, P. C. & Schramm, V. L. (2007). *J. Am. Chem. Soc.* **129**, 6984–6985.

The CAZypedia Consortium (2017). *Glycobiology*, **28**, 3–8.

Torney, F., Moeller, L., Scarpa, A. & Wang, K. (2007). *Curr. Opin. Biotechnol.* **18**, 193–199.

Weil, C. E., Burch, R. J. & Van Dyk, J. W. (1954). *Cereal Chem.* **31**, 510–518.

Whelan, W. J. (1971). *Biochem. J.* **122**, 609–622.

Wolfenden, R., Lu, X. D. & Young, G. (1998). *J. Am. Chem. Soc.* **120**, 6814–6815.

Xu, Q.-S., Yan, Y.-S. & Feng, J.-X. (2016). *Biotechnol. Biofuels*, **9**, 216.